AIP Advances

Phase transformation in crystal and magnetic structure and improved dielectric and magnetic properties of Ho substituted $BiFeO_3$multiferroics

Cite as: AIP Advances **9**, 025110 (2019); https://doi.org/10.1063/1.5082386
Submitted: 21 November 2018 . Accepted: 01 February 2019 . Published Online: 13 February 2019

Jogender Singh, Ashish Agarwal, Sujata Sanghi, Pulkit Prakash, A. Das, C. L. Prajapat, and Manisha Rangi

Phase transformation in crystal and magnetic structure and improved dielectric and magnetic properties of Ho substituted $BiFeO_3$multiferroics

Cite as: AIP Advances 9, 025110 (2019); doi: 10.1063/1.5082386
Submitted: 21 November 2018 • Accepted: 1 February 2019 •
Published Online: 13 February 2019

Jogender Singh,[1] Ashish Agarwal,[1,a)] Sujata Sanghi,[1] Pulkit Prakash,[2] A. Das,[2,3] C. L. Prajapat,[4] and Manisha Rangi[5]

AFFILIATIONS

[1]Department of Physics, Guru Jambheshwar University of Science & Technology, Hisar 125001, Haryana, India
[2]Solid State Physics Division, Bhabha Atomic Research Centre, Mumbai 400085, India
[3]Homi Bhabha National Institute, Mumbai 400094, India
[4]Technical Physics Division, Bhabha Atomic Research Centre, Mumbai 400085, India
[5]Department of Physics, Vaish College, Rohtak 124001, India

[a)]**Corresponding author**: *Ashish Agarwal* **Email:** aagju@yahoo.com **Tel.:** +91-1662-263384; **Fax:** +91-1662-276240.

ABSTRACT

The changes in crystal and magnetic structure of $BiFeO_3$ produced by partial substitution of Bi ions by Ho ions has been studied with powder X-ray diffraction, neutron powder diffraction, dielectric and magnetization techniques. The present study demonstrates that $Bi_{1-x}Ho_xFeO_3$(x = 0.05, 0.10, 0.15, & 0.2) multiferroics shows change in crystal structure at x > 0.05. The sample with x = 0.05 exhibits rhombohedral structure (space group R3c), while the other three samples (x > 0.05) exhibit mixed phase with coexisting rhombohedral (R3c) and Orthorhombic (Pnma) structure. This change in the crystal structure is attributed to the distortion of FeO_6 octahedra via substitution of Ho at phase boundaries. The magnetization studies indicate that doping of Ho in pristine $BiFeO_3$ leads to enhancement in the ferromagnetic moment. We find that doping of Ho breaks the spin cycloid phase of $BiFeO_3$ and creates a canted G-type antiferromagnetic structure in the hexagonal phase whereas the orthorhombic phase exhibits a collinear G-type AFM structure. The canting angle increases with increase in doping with Ho, leading to an enhancement in the ferromagnetic component in magnetization. Dielectric constant (ε′) and loss factor (tanδ) are measured in frequency range 1 kHz to 7 MHz and ε′ and tanδ show dispersion behaviour at low frequencies. The significant improvement in magnetization and dielectric properties is achieved by Ho substitution which in turn enhances the potential of $BiFeO_3$ for multiferroics applications.

I. INTRODUCTION

Multiferroic compounds have been paid a lot of attention due to their attractive basic physics and industrial applications in magnetic/ferroelectric systems used as data storage devices, sensor devices, electromagnets, quantum and spintronics.[1–3] $BiFeO_3$ (BFO) is one of the most widely studied room temperature (RT) single phase multiferroic ceramic, because it has ferroelectric order below a high Curie temperature (T_C ~1103 K)[4,5] and the G-type antiferromagnetic parameters ordering of the Fe magnetic moments below a high Néel temperature (T_N = 643 K).[5] The G-type magnetic structure has been modified by a long-wavelength (λ~ 620 Å) spiral modulation associated with a canting of magnetic moments.[6,7] In this compound, the ferroelectricity is induced by a stereo-chemically active $6s^2$ lone pair of the Bi^{3+} ions. The pure $BiFeO_3$ is described with a polar rhombohedrally distorted perovskite ABO_3 structure with space

group R3c.[8] It has been reported that the space group R3c allows the appearance of the linear magneto-electric effect in $BiFeO_3$ although, the spin modulated spin structure (SMSS) excludes it, and only the quadratic magneto-electric effect was found in $BiFeO_3$.[9,10] The SMSS also exists at temperatures near the Neel temperature.[11] Near the transition temperatures the magnetic long-period modulated structures usually become collinear.[12] It has been shown by Sosnowska et al.,[13] that the SMSS in $BiFeO_3$ can be described by anisotropic relativistic interactions. The ^{57}Fe NMR investigation of $BiFeO_3$[14] confirmed the model calculations of the SMSS arrangement as confirmed by Sosnowska et al.[13] Along with SMSS arrangement, existence of the secondary phases such as $Bi_2Fe_4O_9$ and $Bi_{25}Fe_2O_{39}$ in BFO which causes high current leakage and low resistivity are also the hindrance in practical use of BFO.[14,15] To overcome these problems many solutions have been tried by several groups but substitution method are found to be the best to change specific physical properties of a material. Substitution can be done at Bi site by rare earth divalent ion and Fe site by transition metal ion.[16–18] There are many reports on the rare earth doped BFO, such as La, Gd, Sm, which are found to be helpful in the formation of single phase $BiFeO_3$, suppresses the secondary phases and reduce the leakage current. Due to the maximum magnetic moment ($10.6\mu_B$) of Holmium (Ho) among rare earth elements its substitution will play very interesting role. Partially replacing Bi ions in $BiFeO_3$ by Ho ions lead to a first order magnetoelectric effect in $BiFeO_3$.[19] Previous studies on Ho doped $BiFeO_3$[20] show a structural transformation from Rhombohedral to Orthorhombic and enhancement in the magnetization. However, the role of Ho on the disappearance of cycloid magnetic ordering and appearance of improved magnetization has not been addressed. Similar structural phase transformation from rhombohedral to orthorhombic has also been observed in the $Bi_{1-x}Ca_xFeO_3$ compound[21,22] and enhancement in the magnetization with Y doping and La doping[23] leading to change in multiferroics characteristics has been reported. In this manuscript we investigate the changes in the chemical and magnetic structure using neutron diffraction and other techniques and show the appearance of canted antiferromagnetic structure with Ho doping. The canting angle progressively increases with Ho doping. The results are compared with existing doping studies with trivalent ions and the effect of external pressure on $BiFeO_3$.

II. EXPERIMENTAL

Polycrystalline samples of $Bi_{1-x}Ho_xFeO_3$(x = 0.05, 0.10, 0.15 and 0.20 and henceforth designated as H05, H10, H15, and H20 respectively) were synthesized by solid state reaction route using high purity oxide powders of Bi_2O_3, Ho_2O_3 and Fe_2O_3 from Sigma Aldrich. All the chemicals were weighed in stoichiometric amounts, mixed thoroughly and homogenized using agate mortar with pestle till a uniform mixture was obtained and sintered for 30 minutes at 820°C in an alumina crucible. X-ray diffraction (XRD) spectra were recorded at room temperature using Rigaku Miniflex-II diffractometer with Cu K_αx-ray with the scanning rate of 2°/minute and 2θ ranged from 20° to 80°.Si powder was used as the standard sample for calibration and correcting the zero-point shift in the measured X-ray diffraction patterns. Neutron diffraction (ND) patterns at several temperatures below 300Kwere recorded on the PD2 powder diffractometer (λ=1.2443 Å) in Dhruva reactor Mumbai. The micro-Raman spectra were measured using Raman spectrometer (Enspectr Enhanced spectroscopy, USA) with a green excitation light source of 532nm. Rietveld refinement of the data were analysed using FullProf program.[24] Structural properties have been obtained from the analysis of both X-ray and neutron diffraction pattern. Micrographs of samples were recorded using JEOL scanning microscope (SEM). Magnetic properties of the multiferroic samples were measured at room temperature with Vibrating Sample Magnetometer and SQUID magnetometer (Quantum design, MPMS5) at low temperature (5K-300K). For dielectric measurements the solid discs of the samples were made by applying a pressure using a pellet press at room temperature. For proper shaping, poly vinyl alcohol (PVA) was used as a binder agent. The prepared pellets are of about 10 mm diameter and 1 mm thickness. For making electrodes two surfaces of the sintered discs were coated with silver paste. Dielectric measurements were performed with an impedance/gain phase analyser (Newton's 4th Ltd) in frequency range 100Hz – 7MHz at different temperature.

III. RESULTS AND DISCUSSION

A. X-ray diffraction

The crystal structure of H05, H10, H15 and H20 compounds was analysed using X-ray and neutron diffraction techniques. The absence of the impurity phases in the XRD pattern means that doping Ho restricts the impurity phases to grow that exist in pristine $BiFeO_3$ solid solution. As the concentration of Ho is enhanced, splitting of main peak at ~ 32° is reduced and an extra peak grows at around 25° indicating a coexistence of hexagonal and orthorhombic structure. The analysis of the room temperature XRD patterns taking into account both the hexagonal and orthorhombic phases were carried out using FullProf software. Rietveld refined XRD patterns of H05, H10, H15 & H20 are shown in Figure 1 Good agreement between the observed and calculated pattern is obtained in all the samples. Pure $BiFeO_3$ crystallizes with a rhombohedral structure (space group R3c).[25] For the sample H05, refinement of XRD pattern is performed assuming R3c space group as an initial model. The background parameters were fitted using Fourier cosine series and peak shapes were fitted by pseudo-Voigt function. All the peaks were reproduced in the refinement, which confirms that no change in structure occurs for H05 substitution of Ho. As the concentration of Ho is increased for H10, all the peaks were not reproduced by symmetry R3c which points towards the mix phase. The XRD pattern of H10 sample, was found to fit best by 2 phase refinement including rhombohedral (R3c) structure and orthorhombic (Pnma) structure. The cause of the structural transition for H10, may be attributed to mismatch in ionic radii of host Bi and doped Ho ion. The smaller size

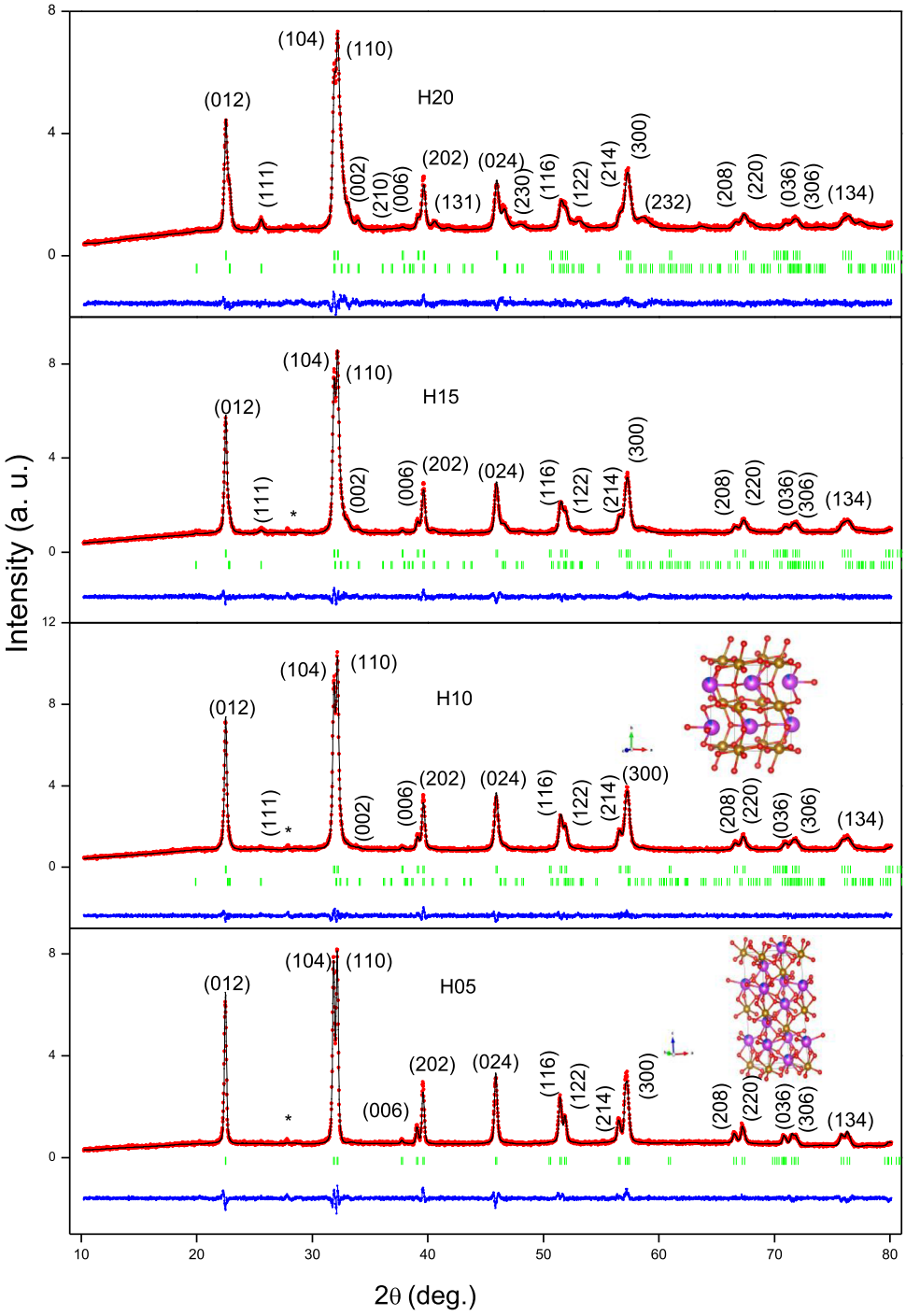

FIG. 1. Rietveld refined XRD patterns of H05, H10, H15 & H20 multiferroics. The tick marks indicate the position of reflections in hexagonal phase (top) and orthorhombic phase (bottom). The inset shows the structure in the hexagonal and orthorhombic phase.

of Ho^{3+} ion (0.901 Å) as compared to Bi^{3+}ion (1.03Å) produces strain in the lattice. This disturbs the FeO_6 octahedral leading to transformation in crystal structure.[15] For H15 & H20 samples, refinement was done by the combination of hexagonal and orthorhombic structures which reproduces all the observed peaks. The lattice parameters and volume decrease with increasing Ho content is due to the smaller size of Ho than Bi. The structural parameters obtained from this analysis are used as the starting model for the analysis of neutron diffraction patterns discussed next.

B. Neutron diffraction

The neutron powder diffraction (ND) patterns were recorded at several temperatures below 300K for all the samples in the series $Bi_{1-x}Ho_xFeO_3$ with H05, H10, H15& H20. At all temperatures 300K and below, strong super lattice reflection (003) (101) is observed (indicated in Figure 2) establishing the antiferromagnetic nature of the sample. The parameters obtained from XRD were used as the starting model for refining the neutron diffraction patterns. In hexagonal structure (R3c, space group No. 161) Bi and Fe occupies 6(a) (0,0,z) Wyckoff position and O occupies 18(b) (x,y,z) position. Here the position of the atoms, occupancy, and thermal parameters are varied. Rietveld refined ND pattern of all sample at 6K is shown in Figure 2. The crystal structure of the compound H05 has been refined in a single phase polar R3c space group. The best fit for samples with x > 0.05 is obtained by considering two phases with rhombohedral (R3c) and orthorhombic (Pnma) structures. The unit cell volume of both the hexagonal and orthorhombic phases decrease with increase in x. For low Ho concentration the orthorhombic phase fraction is very low and therefore the parameters are subject to greater error. The variation of the unit cell volume with x is shown in Figure 3. The volume fraction of the orthorhombic phase increases with increase in Ho doping. Our results differ from the earlier published result[20] on the same series, where it is shown that the compound undergoes a complete transformation to the orthorhombic phase for H20, whereas we observe coexistence of the two phases. The neutron diffraction data confirm that at low temperature there is no further change in crystal structure which shows its structural stability with temperature. The crystal structure parameters obtained from Rietveld refinement of powder XRD and powder neutron diffraction patterns are in good agreement and are summarised in Table I.

C. Magnetic properties

Figure 4 shows the temperature variation of magnetization (M) in both ZFC and (FC) state at H=1kOe for all the samples. The magnetization decreases with lowering of temperature from RT to 105K and below ~100K it sharply increases. Similar anomalous behaviour in M (T) has also been reported earlier in Ho doped[20] and Gd doped BiFeO3.[26] In the latter reference the rapid rise below ~100K has been attributed to magnetic ordering of Gd^{3+} ions. The anomalous behaviour is observed only in H10 and H15 samples in our case. However, in our neutron diffraction experiments, discussed later, we are unable to find a signature for this behaviour. As observed from our neutron diffraction studies there are neither evidences of spin reorientation of the Fe moments, as suggested in single crystal studies of $BiFeO_3$[27] at this temperature nor the Ho moments magnetically order below this temperature. We attribute this behaviour to the interplay between Ho paramagnetic moments and antiferromagnetic behaviour of $BiFO_3$. The lowering of the M(T) on reduction of temperature arises from the antiferromagnetic nature of the sample. We attribute the observed minimum in M(T) to the interplay between Ho

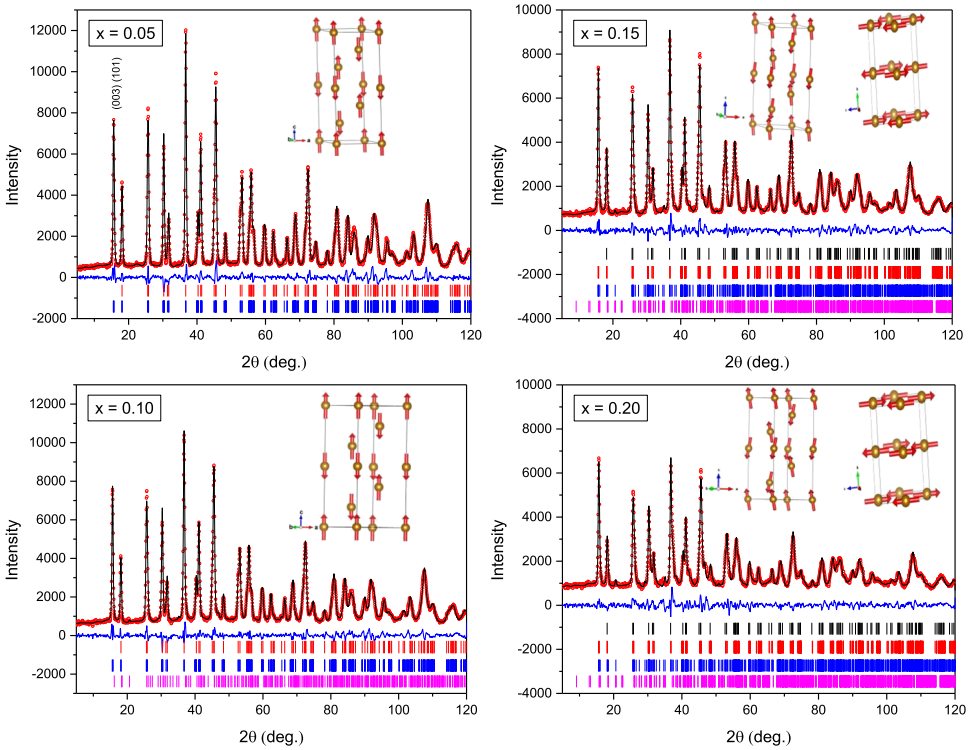

FIG. 2. Rietveld Refinement of neutron diffraction of $Bi_{1-x}Ho_xFeO_3$ (x = 0.05, 0.10, 0.15 and 0.20) at 6K.

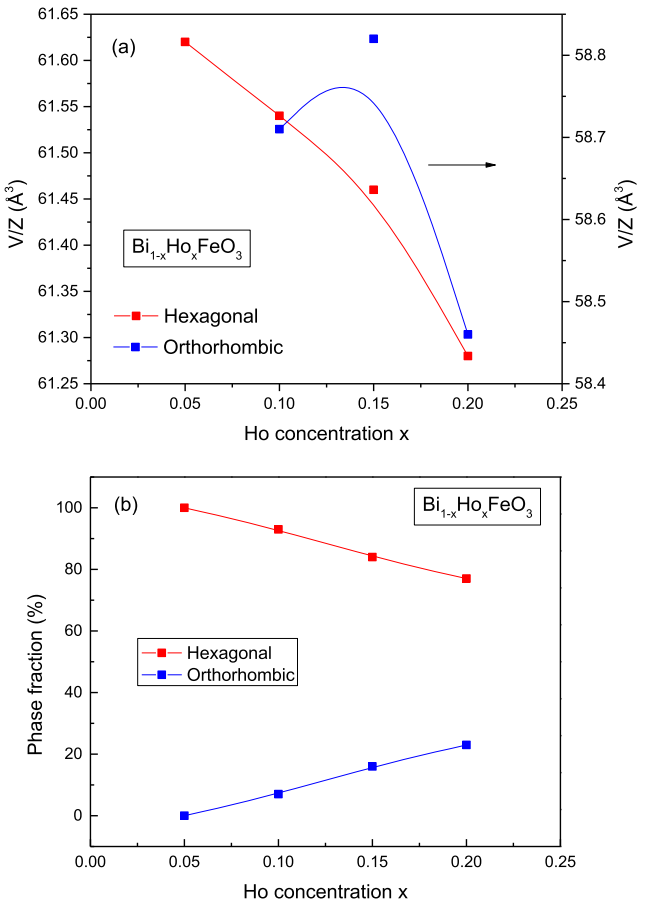

FIG. 3. (a) Variation of unit cell Volume (b) phase fraction of the series $Bi_{1-x}Ho_xFeO_3$ with concentration of Ho (x).

paramagnetic moments and antiferromagnetic behaviour of $BiFO_3$. There appears a small hysteresis between ZFC and FC curves below 25K in all the doped samples. This coincides with the spin glass temperature ~ 29K reported in $BiFeO_3$.[27] Similarly, spin glass behaviour has also been observed in $0.3NiFe_2O_4$-$0.7BiFeO_3$ nanocomposites.[28]

The variation of magnetization with field for all the samples at 5K and 300K is shown in Figure 5. The samples do not show any hysteresis or H_C at 300K and 5K confirming its antiferromagnetic nature. For samples with x>0.05 ferromagnetic like hysteresis behaviour is observed at 5K. Though a clear square hysteresis loop is observed only for the sample H10 indicating a ferromagnetic behaviour. The large slope in the M(H) curves at high fields and hysteresis loops in the low fields indicates a canted antiferromagnetic behaviour which we establish from the neutron diffraction experiments. Due to increase in Ho concentration, there are new additional magnetic interactions such as Ho-Ho and Ho-Fe in addition to the regular Fe-Fe interaction.[29]

From the Figure 5(a) we can see a small residual magnetism is observed. There is a gradual increase in curvature of M-H loops approaching towards saturation with increase the Ho part at A- site in BFO. The magnetization at 50 kOe increases from 5.07 emu/g for H05 to 9.60 emu/g for H10 at 5K. Further, it is increases systematically with increase of Ho part and reaches a maximum value of 15.9emu/g which are also confirmed by the neutron diffraction magnetic parameters.

Figure 5(b) Represent the room temperature behaviour of M-H loop with a maximum field of ±60 kOe.

The neutron diffraction pattern shown in Figure 2 indicates strong super lattice reflection (003) (101) in addition to nuclear reflections at 6K. On heating to 300K, the intensity of this reflection reduces marginally, which is in agreement with T_N for this compound is at a much higher temperature than 300K. The reflections were indexed in R-1 space group with propagation vector $\mathbf{k}$ = 0. The basis vectors were obtained using Sarah program.[30] The magnetic structure is modelled with moment on Fe site alone. No signature of magnetic ordering of Ho was evident in our analysis. In H05 and H10 samples, collinear G-type antiferromagnetic structure is observed. The magnetic moment is oriented along the hexagonal c axis and its value ~4.3μ_B is close to the value of 5μ_B expected for Fe^{3+} (S = 5/2) ion. In H10 sample, the orthorhombic phase is found to be paramagnetic. It is also possible that the signature of magnetic ordering of the orthorhombic phase is not detectable in our neutron diffraction experiment due to small phase fraction of the orthorhombic phase. With increase in Ho, for samples with 15% and 20% Ho, a further enhancement in the intensity of (101) reflection is observed. This could not be accounted for by taking moment on Fe in the hexagonal phase alone. This was modelled taking into consideration the magnetic ordering of Fe in both the hexagonal and orthorhombic phases. In H15 and H20 samples, magnetic structure of the hexagonal phase shows canted G- type AFM structure while the orthorhombic phase is found to be collinear G-type AFM. These magnetic structures are shown in inset to Figure 2. The value of FM and AFM moments are summarized in Table I. The values of ferromagnetic moment (FM) in hexagonal phase increases from zero to 1.3 μ_B with increase in the Ho concentration at A site and the resulting orthorhombic structure. The canting angle of the Fe moments (FM moment) in hexagonal phase increases with increase in the orthorhombic phase. The increase in the canting of the moments in hexagonal phase with increase in volume fraction of the orthorhombic phase could be due to the strain induced in the lattice. The effect of the external pressure on $BiFeO_3$ shows the sample undergoes a structural transition from hexagonal to orthorhombic via an intermediate monoclinic phase at 10GPa.[31] Similarly, an increase in the magnetic susceptibility χ under pressure is observed and has been ascribed to increased hybridization between Fe(d) and O(2p) states.[32] Thus the emergence of the orthorhombic phase and spin canting behaviour in our sample plausibly indicates the effect of doping Ho plays a role similar to the external pressure. However, the pressures reached by doping are much smaller than the external pressure as indicated by the value of $c/a\sqrt{6}$ is only 1.012 in our H20 sample as against reported value of 1.0048 at 3.4GPa external pressure.[31] The enhanced magnetization in Ho doped $BiFeO_3$ reported earlier[20] and

TABLE I. Refined structural parameters, Bond Length and Bond Angle of H05, H10, H15 & H20 samples obtained from analysis of Neutron Diffraction Patterns at 6K.

	0.05	0.10		0.15		0.20	
	R3c	R3c	Pnma	R3c	Pnma	R3c	Pnma
a(Å)	5.56087(15)	5.5580(2)	5.588(4)	5.5574(3)	5.553(19)	5.5531(4)	5.5436(15)
b(Å)	5.56087(15)	5.5580(2)	7.816(3)	5.5574(3)	7.821(3)	5.5531(4)	7.805(2)
c(Å)	13.807(8)	13.801(10)	5.377(3)	13.788(12)	5.417(19)	13.767(17)	5.4042(15)
V/Z ($Å^{-3}$)	61.62	61.54	58.71	61.46	58.82	61.28	58.46
Volume Fraction (%)		93	07	84	16	77	23
Bi/Ho							
x	0.0000	0.0000	0.011(6)	0.0000	-0.001(3)	0.0000	-0.006(3)
y	0.0000	0.0000	0.2500	0.0000	0.2500	0.0000	0.2500
z	0.2209(14)	0.2212(14)	-0.033(5)	0.2216(16)	-0.036(2)	0.2220(2)	-0.0380(18)
B_{iso} ($Å^2$)	-0.01	0.01	0.5	0.01	0.5000	0.01	0.5
Fe							
x	0.0000	0.0000	0.0000	0.0000	0.0000	0.0000	0.0000
y	0.0000	0.0000	0.0000	0.0000	0.0000	0.0000	0.0000
z	0.0000	0.0000	0.5000	0.0000	0.5000	0.0000	0.5000
B_{iso} ($Å^2$)	0.17	0.14	0.5	0.19	0.5	0.25	0.5
O							
x	0.8888(5)	0.8886(5)	-	0.8891(6)	-	0.8880(9)	-
y	0.6466(5)	0.6472(5)	-	0.6482(6)	-	0.6493(9)	-
z	0.4354(2)	0.4352(2)	-	0.4354(2)	-	0.4369(4)	-
B_{iso} ($Å^2$)	0.50	0.55	-	0.50	-	0.59	-
O1							
x	-	-	0.629(9)	-	0.624(4)	-	0.628(3)
y	-	-	0.2500	-	0.2500	-	0.2500
z	-	-	0.066(8)	-	0.054(4)	-	0.069(3)
B_{iso} ($Å^2$)	-	-	0.5000	-	0.5000	-	0.5000
O2							
x	-	-	0.304(6)	-	0.294(3)	-	0.2949(19)
y	-	-	0.044(4)	-	0.025(2)	-	0.0292(15)
z	-	-	-0.320(6)	-	-0.307(2)	-	-0.2983(18)
B_{iso} ($Å^2$)	-	-	0.5	-	0.5	-	0.5
M (μ_B) (AFM)	4.1(1)	4.3(1)	-	4.25(2)	4.7(2)	4.7(2)	4.7(2)
M (μ_B) (FM)	-	-	-	1.0(2)	-	1.3(2)	-
Bi/Ho-O(Å)	2.507	2.506	-	2.505	-	2.515	-
Bi/Ho-O1(Å)	-	-	2.94	-	2.89	-	2.964
Bi/Ho-O2(Å)	-	-	2.77	-	2.811	-	2.792
O-Bi/Ho-O(deg)	145	144.8	-	144.8	-	145.2	-
O1-Bi/Ho-O1(deg)	-	-	152	-	151.2	-	149.2
O2-Bi/Ho-O2(deg)	-	-	124	-	125.7	-	174.2
O1-Bi/Ho-O2(deg)	-	-	135	-	133.1	-	135.7
Fe-O-Fe (deg.)	154.22	154.50		154.70		154.43	
Fe-O (Å)	1.956	1.953		1.949		1.927	
Fe-O (Å)	2.096	2.094		2.096		2.117	
χ^2	5.99	4.41		4.29		4.79	
R_{Bragg}(%)	3.13	3.07	9.02	2.36	6.21	3.55	7.23

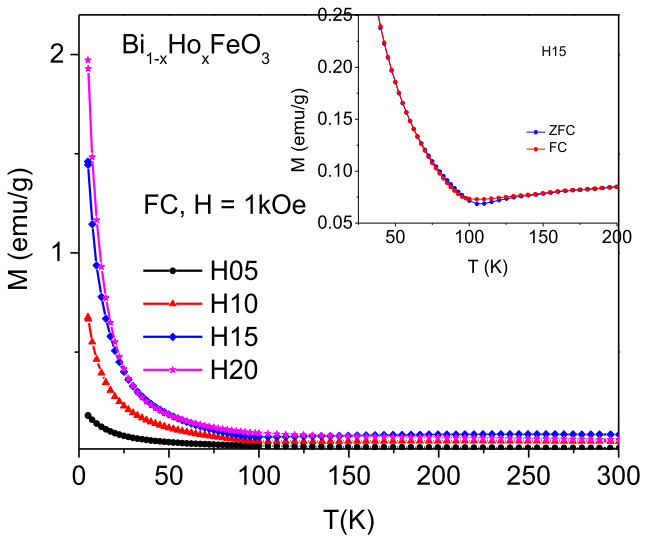

FIG. 4. Temperature variation of magnetization in FC state measured in H=1kOe, for H05, H10, H15 & H20 samples. The inset shows the same in a magnified scale for the sample H15 in ZFC and FC state.

which we too observe in our magnetization studies arises from the increased canting of the G-type AFM spins as a result of Ho doping.

D. Raman spectroscopy

Figure 6 shows the deconvoluted micro-Raman spectra for all the samples at room temperature. The micro-Raman scattering is responsive to vibrations of lattice in crystal structure and it can be used effectively for collecting information about the micro structural description of lattice in present samples. The peak of each component, i.e., the natural frequencies of active modes of Raman spectrum, was observed in all the samples. The deconvolution into individual Lorentzian components was done using OriginPro (Table II). There can be 13 optical-phonon active modes ($4A_1$ + 9E) present in pure $BiFeO_3$ for rhombohedral R3c symmetry as per group theory. But the observed spectrums feature of BHFO give only few fundamental Raman modes, broadening and shifting of some A1 and E modes. Due to significant difference in atomic weights of Ho (164.93 g/mol) and Bi (208.98 g/mol) BHFO shows sign of hardening A1 modes at lower frequencies which plays important role for covalent bonding of Bi-O.[16] It is pertinent to mention that the doping of Ho in BFO may disturb central symmetry of the compound, which is further responsible for lowering the stability of compound, resulting from the stereo chemical reduction process of Bi $6s^2$ electrons because of the spherical distribution of electron density in Ho^{3+} ion. The internal vibration of Fe in octahedral FeO_6 and occupational level of Bi cause associated high and low frequency modes respectively.[20] Literature survey indicate that the obtained results are similar to former reported results for bulk BFO and $Bi_{0.09}Ho_{0.10}FeO_3$ compounds.[15,33,34]

E. Scanning electron microscope (SEM) analysis

Figure 7 depicts series of the scanning electron micrograph (SEM) of samples H05, H10, H15 & H20. All micrographs represent the dense and uniform morphology of the samples. The microstructure analysis of these samples reveals the size of grains reduces with increase of Ho doping. The reduction in the grain size enhances the density of samples which causes enhancement in resistivity of prepared ceramics. It signifies that Ho doping suppress the growth of grains which resulting in small grain sizes of highly doped samples reflects in the SEM micrographs of sample H10. Another possible reason of decrease in grain sizes is the dissimilarity in the ionic radius of Bi^{3+} and Ho^{3+}. Kirkendall effect[35] might be the alternative reason for decrement in grain size with doping which arose because of the difference in the diffusion rates of constituent elements of the prepared compounds. Earlier studies suggested that the reduction in the grain size is ascribed to the suppression of oxygen vacancies with the Ho doping. Since the motion of oxygen vacancies during the sintering mechanism are responsible for grow with of grains.[36]

F. Dielectric study

The dielectric properties depend on frequency and oscillation of dipole with the direction of the applied electric field.[37] Figure 8 represents the frequency dependence of real part of dielectric constant (ε′) and dielectric loss (tanδ) (inset) for all the samples H05, H10, H15 & H20 at various temperatures. Figure 8 shows that for all the samples the behaviour of dielectric constant is nearly same. The dielectric constant (ε′) and dielectric loss (tanδ) at lower frequency display a large dispersion and become nearly constant at higher frequency. This type of behaviour at low frequency may be attributed to the interfacial dislocations, oxygen vacancies, grain boundary effect etc. as at high frequency both applied external field and charge carriers are not in same direction. It is explained on the basis of Maxwell-Wagner model[15,36,38] and Koop's theory.[39] According to Maxwell-Wagner model, polycrystalline materials possess well conducting layers of grains that are separated by highly resistive grain boundaries. When an electric current is passed through the dielectric material, then there is a formation of space charge polarization around the grain boundaries. The switching of electrons between ions of same element[25] is also involved in this polarization mechanism. In the samples under study, switching of electrons takes place between Fe^{3+} and Fe^{2+} ions. The electrons pass through grains and grain boundaries during this exchange but due to high resistance of grain boundaries, the electrons build up at grain boundaries and which results in space charge polarization. In low frequency region, the dielectric constant increases suddenly and becomes low in high frequency region, because of high resistance offered by the grain boundaries in low frequency region. Therefore, more energy is required for the movement of charge carriers which leads to high dissipation of energy in this region.[40] Whereas, in high frequency region, low resistance is applied by the grains and therefore, less energy is needed for the movement of charge carriers and energy loss is small.[41]

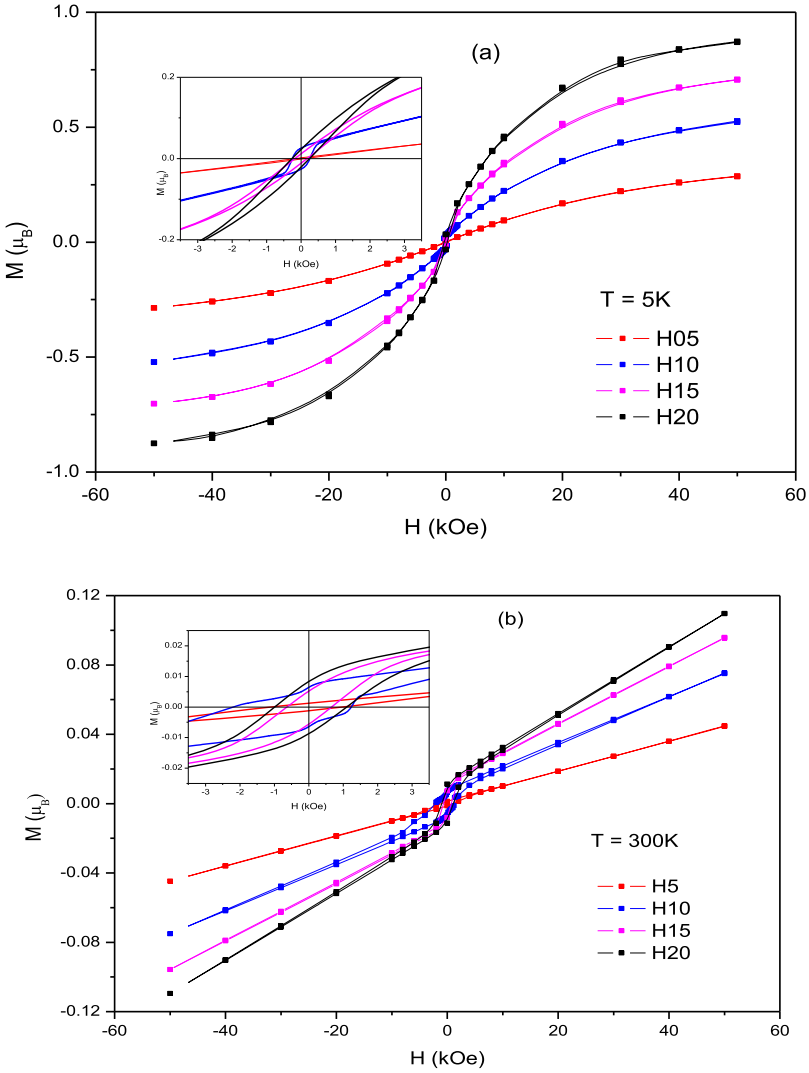

FIG. 5. (a) The variation of magnetization with magnetic field for all the compounds at 5K (b) at 300K.

Variation of dielectric loss (tanδ) with frequency is similar to the variation in dielectric constant for all the prepared samples. The frequency dependent region of dielectric constant reduces with increasing Ho percentage as shown in Figure 8 as Ho has a higher valence as compared to Fe and thus substitution of Ho restrains the oxygen vacancies due to charge compensation phenomenon. As the concentration of Ho is increased, the dielectric constant increases, which shows that Ho^{3+} substitution improves the dielectric properties of $BiFeO_3$ ceramics.

Figure 9 shows the variations of dielectric constant and dielectric loss (tanδ) of the $Bi_{0.95}Ho_{0.05}FeO_3$ (representative figure of the samples) ceramics as a function of temperature at different frequencies. All the samples follow similar behaviour. The value of permittivity is high at high temperature this is in accordance to Maxwell-Wagner polarization phenomenon.[42–44] There are two permittivity anonymous peaks (at 1 kHz) which also disappear with increase in frequency in the temperature range 450-650K. The peak at 450K may be caused by formation defects (during sintering), whereas the peak around 650K could be due to the antiferromagnetic phase transition.[45,46] The ferromagnetic behaviour in the compound results in high value of permittivity. Inset in the Figure 9 displays the temperature dependent dielectric loss in which the behaviour of spectrum is similar to dielectric constants. The dipole fatalities contribute to loss in permittivity followed by conduction of smooth curve. Numerous kind of loss phenomenon are further attributed to dielectric loss. The contribution of dipole loss attains a maximum value at certain temperature and start decreasing with further increase in temperature. Due to constraints at instrumentation part we are unable to extend the temperature range. In the implemented temperature range we can conclude that although the dielectric loss has low value in the beginning but it increases significantly with increase in temperature.

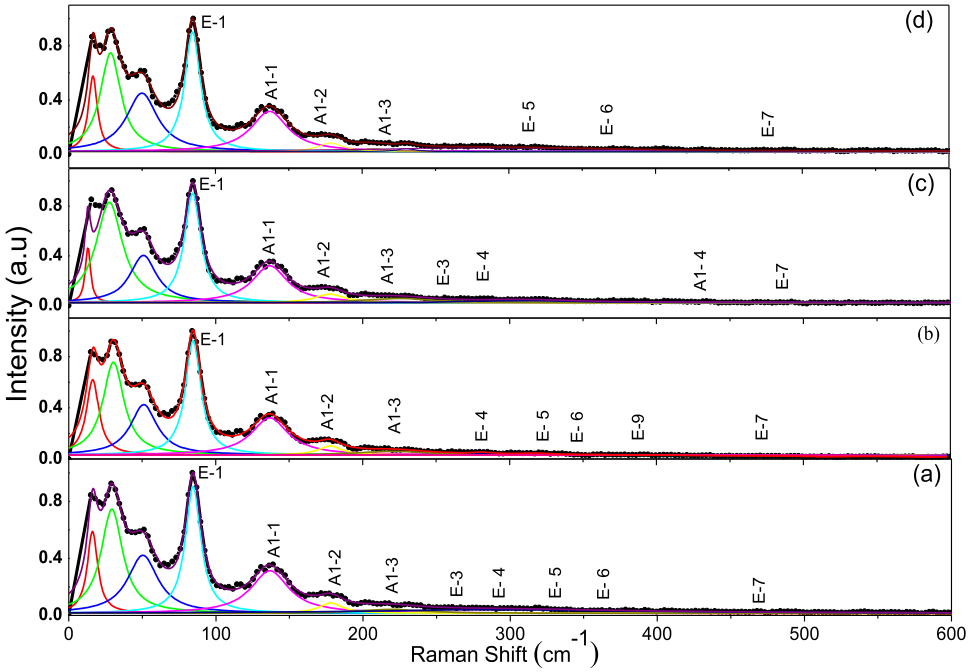

FIG. 6. The micro-Raman spectra of $Bi_{1-x}Ho_xFeO_3$ ceramic: (a) H05; (b) H10; (c) H15; (d) H20.

TABLE II. Raman modes for deconvoluted Raman spectra.

	Observed study					
	$(Bi_{1-x}Ho_xFeO_3)$ BFO Bulk			$Bi_{0.90}Ho_{0.10}FeO_3$	Literature	
Raman Modes	H05	H10	H15	H20	32	33
A1-1	136.72	136.76	136.77	136.84	135.15	142
A1-2	178.03	177.84	177.73	178.37	167.08	173
A1-3	218.03	221.09	224.54	230.09	218.11	228
A1-4	-----	-----	434.25	-----	430.95	-----
E-1	84.52	84.64	84.27	84.38	71.39	-----
E-2	-----	-----	-----	-----	98.36	-----
E-3	260.97	-----	255.95	-----	255.38	-----
E-4	294.67	281.72	285.51	-----	283.00	270
E-5	319.93	317.51	-----	317.15	321.47	-----
E-6	362.52	341.81	-----	371.15	351.55	367
E-7	468.01	474.81	491.91	486.99	467.60	471
E-8	-----	-----	-----	-----	526.22	523
E-9	-----	390.30	-----	-----	598.84	-----

G. Impedance analysis

Material's electrical and structural properties can be studied through Impedance spectroscopy (IS). In electrical resistivity the assistance of grains and grain boundaries can be investigated by this method. Nyquist plots for studied samples are shown in Fig. 10 (x = 0.05, 0.10, 0.15 & 0.20). In Nyquist plots, presence of single semi-circular arcs appears due to involvement of grains.[47,48] The Negative Temperature Coefficient of Resistance (NTCR) have been represented by decreasing radius of semi-circular arc with rise in temperature. The non-Debye characteristics of prepared samples can be concluded from the figures as the centre lie below real Z′ axis of these semi-circular arcs.[49,50] Suppression of oxygen vacancies can be confirmed from the Nyquist plot taken at 563K of all the samples (Fig. 11) which shows that impedance increases with increase in Ho doping.

The variation of imaginary part of impedance (Z") with frequency for all samples at different temperatures is shown in Figure 12. With increase in temperature impedance Z" also decreases followed by plots which justify the contribution of electron hoping to the conduction characteristics of the prepared samples. The broad peak for the all samples corresponds to relaxation frequency at respective temperature.

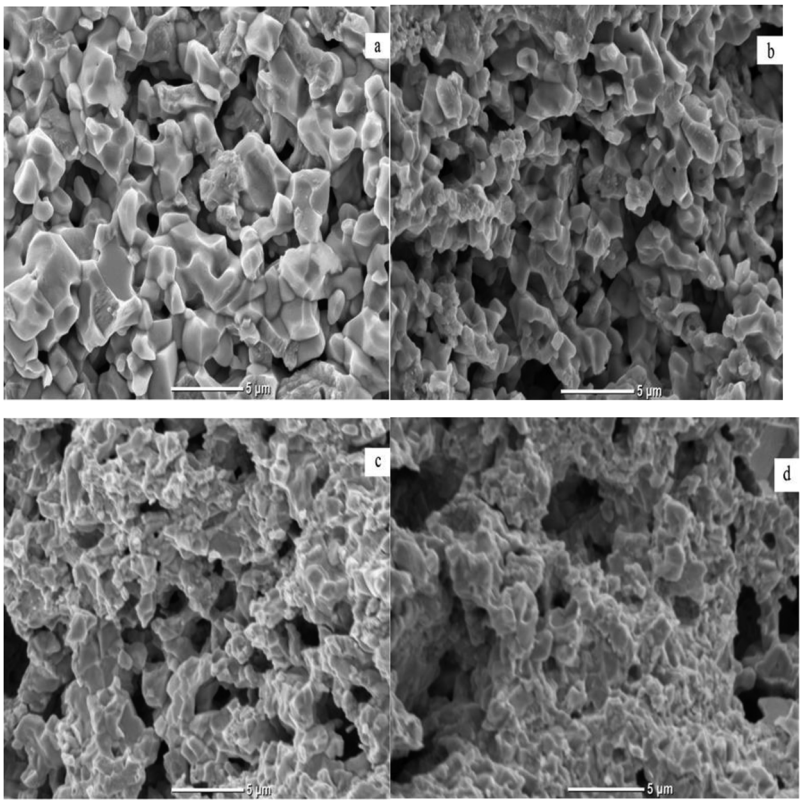

FIG. 7. Surface morphologies of the $Bi_{1-x}Ho_xFeO_3$ ceramics: (a) H05; (b) H10; (c) H15; (d) H20.

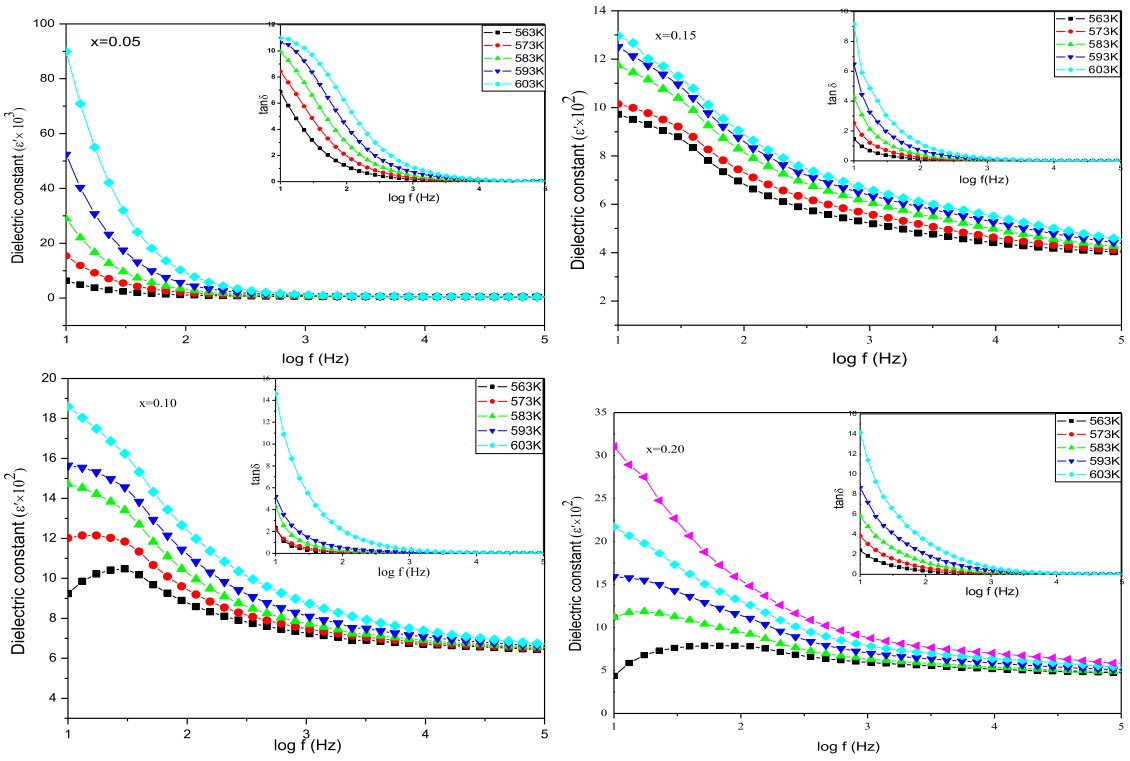

FIG. 8. Variation of dielectric constant and dielectric losses (see inset) with frequency for all the prepared samples at different temperatures.

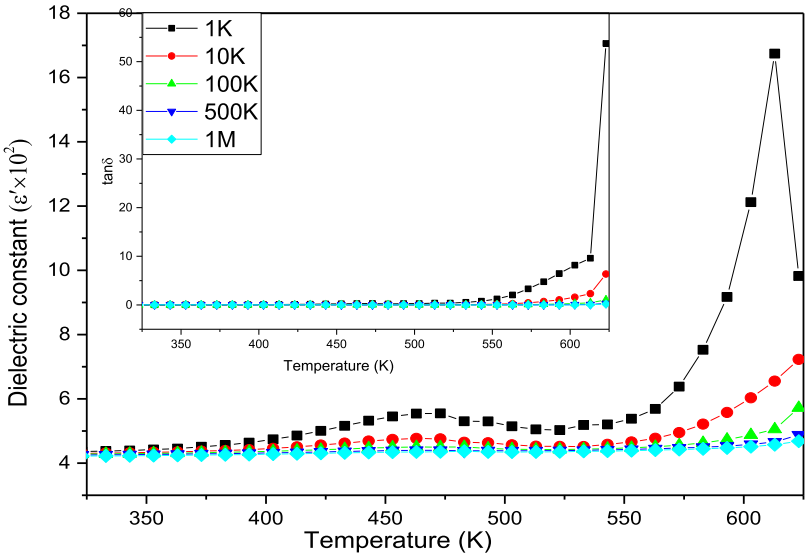

FIG. 9. Variation of dielectric constant and dielectric losses (see inset) with temperatures for $Bi_{0.95}Ho_{0.05}FeO_3$ multiferroics at different frequency.

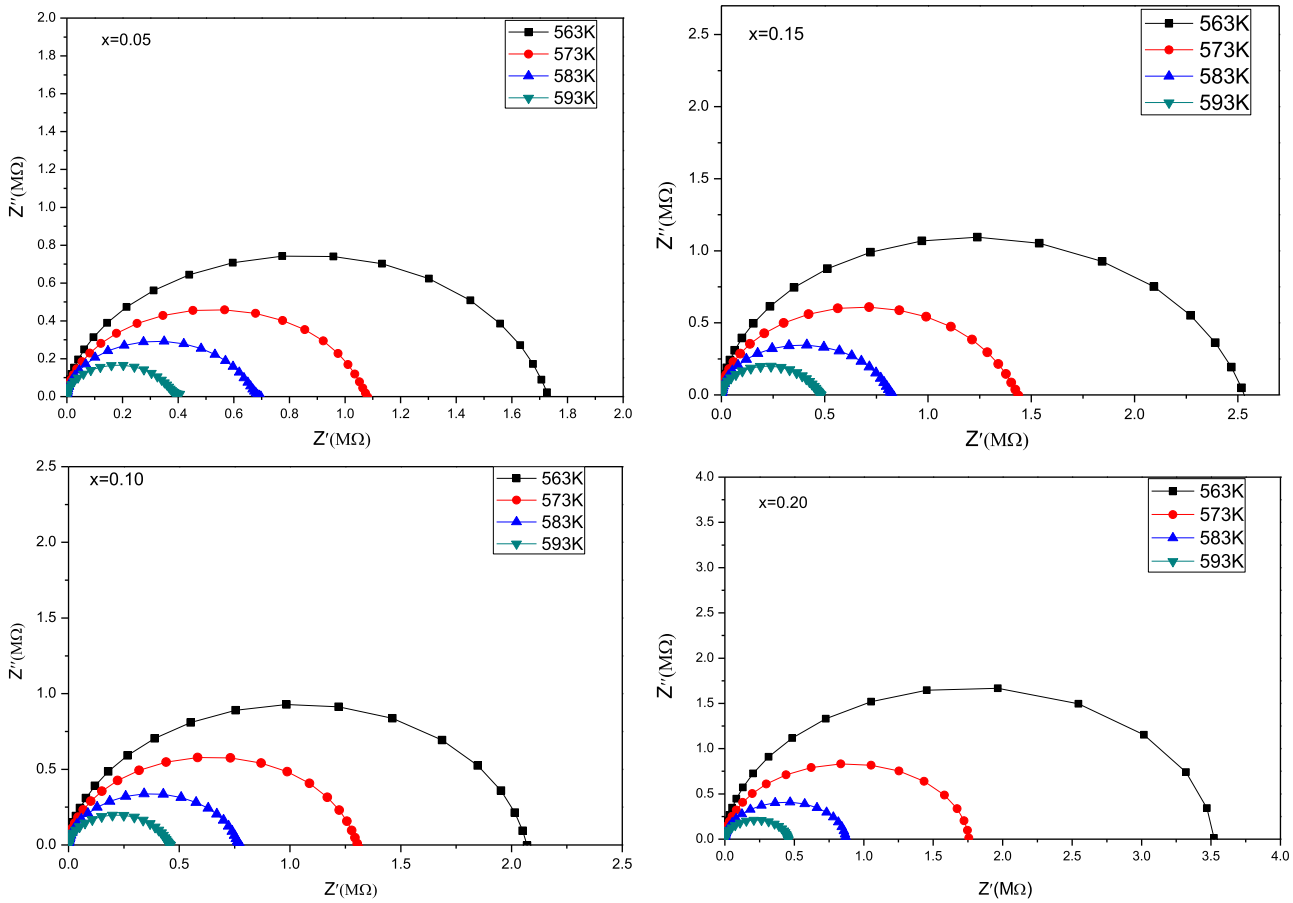

FIG. 10. Nyquist plots for $Bi_{0.90}Ho_{0.10}Fe_{1-x}Ti_xO_3$ multiferroics for all prepared samples at different temperature.

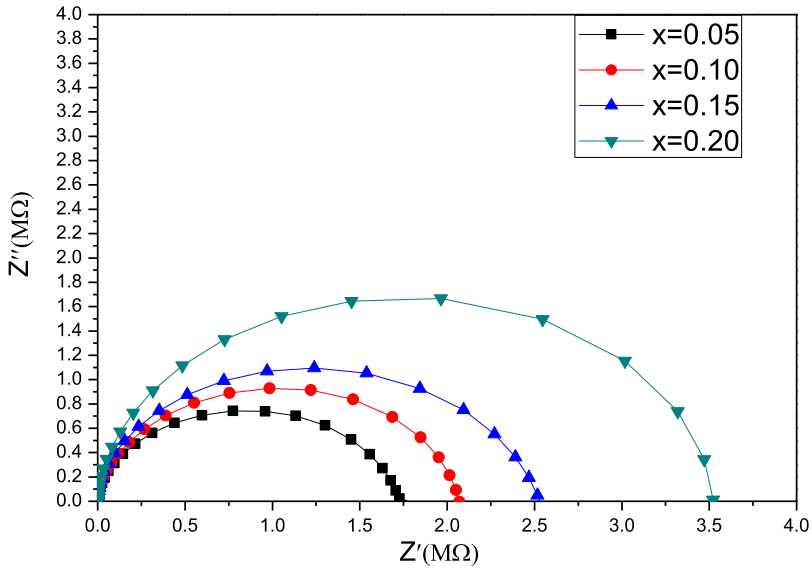

FIG. 11. Nyquist plots for different compositions ae 563K.

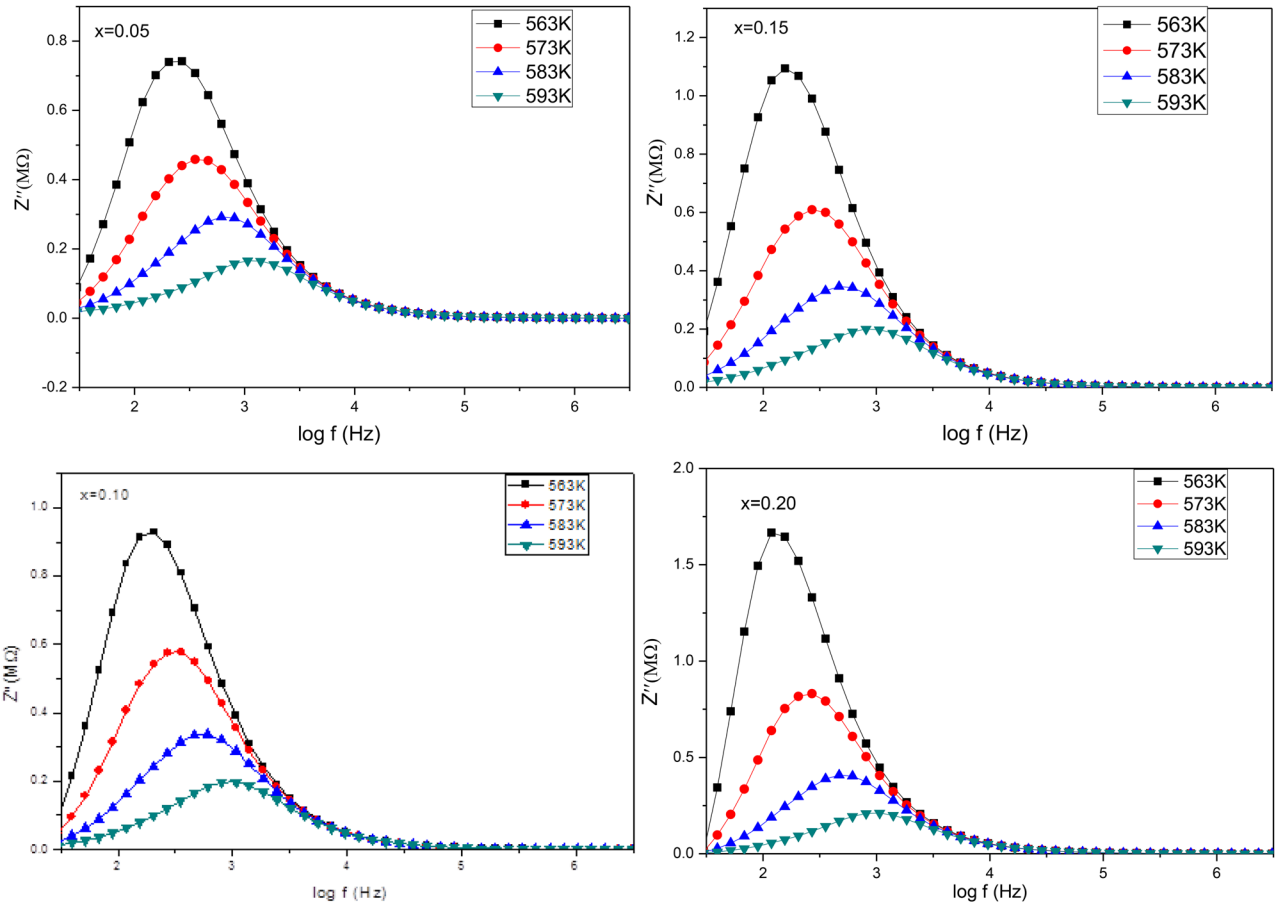

FIG. 12. Variation of imaginary part of resistance (Z") with logarithm frequency (log f).

It can be identified that with increase in temperature the peak get shifted towards higher frequencies and this may be attributed to increase rate of electron hoping. At higher frequencies there is a decrease in polarization due to increase in relaxation time of hoping electron.[51,52] The Arrhenius relation is also satisfied by reciprocal dependence of relaxation time upon temperature.

$$\tau = \tau_o e^{-E_a/k_B T} \quad (1)$$

Where τ_o is pre-exponential factor, E_a is activation energy (in eV), T is the temperature (in Kelvin), k_B is Boltzmann constant and τ is evaluated by using relaxation frequency (f_o) corresponding to maximum value of Z" (from Figure 8) as:

$$\tau = \frac{1}{2\pi f_o} \quad (2)$$

The relaxation time (τ) values calculated using equation (2) are 0.000675s, 0.0008132s, 0.0010208s and 0.0012167s for x=0.05, 0.10, 0.15 and 020 respectively. The calculated values of activation energy (E_a) by using equation (1) are 0.154eV, 0.150eV, 0.145eV and 0.141eV for x = 0.05, 0.10, 0.15 and 0.20 respectively, which indicate that the value of activation energy decreases with increasing doping of Ho.

IV. CONCLUSIONS

Solid state reaction method has been used to synthesize the Ho doped $BiFeO_3$ having composition $Bi_{1-x}Ho_xFeO_3$ with x=0.05, 0.1, 0.15, and 0.20. The crystal structure, magnetic and dielectric properties of these samples have been reported. Powder XRD analysis along with neutron powder diffraction show that samples with x = 0.05 crystallize in rhombohedral structure as that of parent $BiFeO_3$. With increase in concentration of Ho, biphasic system develops, i.e., a combination of rhombohedral and orthorhombic symmetries. The homogeneity of the grain size of different samples have been concluded from SEM Micrographs. For the detailed analysis of magnetic structure at low temperatures, neutron diffraction patterns were recorded and it was observed that there is no change with temperature. With Ho doping, cycloidal spin structure is compressed and uncompensated spin are responsible for ferromagnetic properties. The largest value of magnetization was observed for sample H20, which can be understood by mixed phase structure. Ho doping has improved the dielectric and magnetic properties. Dielectric constant (ε′) and dielectric loss/loss factor (tan δ) show dispersion behaviour in low frequency region. The negative temperature coefficient of resistance in the compound is analysis through Impedance spectroscopy. The structural behaviour indicated that grain and grain boundaries have important role on electrical and structural properties of the compound.

ACKNOWLEDGMENTS

AA and SS acknowledge the Department of Science and Technology, Government of India for providing XRD facility through FIST scheme. J. Singh is thankful to University Grant Commission (UGC), India for providing JRF fellowship. AA and SS are also thankful to DST, New Delhi for providing funds under PURSE program No. SR/PURSE Phase 2/40(G).

REFERENCES

[1] D. C. Arnold, K. S. Knight, F. D. Morrison, and P. Lightfoot, Phys. Rev. Lett. **102**, 027602 (2009).
[2] Y. Tokura, Science **5779**, 1481 (2006).
[3] B. Manuel and B. Agnes, Nature Materials **425**, 7 (2008).
[4] I. Sosnowska, R. Przenioslo, P. Fischer, and V. A. Murashov, J. Magn. Magn. Mater. **160**, 384 (1996).
[5] W. Kaczmarek, Z. Pajak, and M. Połomska, Solid State Commun. **17**, 807 (1975).
[6] I. Levin, S. Karimi, V. Provenzano, C. L. Dennis, H. Wu, T. P. Comyn, T. J. Stevenson, R. I. Smith, and I. M. Reaney, Phys. Rev. B **81**, 020103 (2010).
[7] I. Sosnowska, T. Peterlin-Neumaier, and E. Steichele, J. Phys. C **115**, 4835 (1982).
[8] D. P. Kozlenko, A. A. Belik, A. V. Belushkin, E. V. Lukin, W. G. Marshall, and B. N. S. E. Takayama-Muromachi, Phys. Rev. B **84**, 094108 (2011).
[9] F. Kubel and H. Schmid, Acta Cryst B **46**, 698 (1990).
[10] C. Tabares-Munoz, J.-P. Rivera, A. Bezinges, A. Monnier, and H. Schmid, Jpn. J. Appl. Phys. **24**, 1051 (1985).
[11] I. Sosnowska, M. Loewenhaupt, W. I. F. David, and R. M. Ibberson, Physica B: Condens. Matter **180**, 117 (1992).
[12] I. Sosnowska, W. Schäfer, W. Kockelmann, K. H. Andersen, and I. O. Troyanchuk, Appl Phys.A **74**, 1040 (2002).
[13] I. Sosnowska and A. K. Zvezdin, J. Magn. Magn. Mater **167**, 140 (1995).
[14] F. Xue, Q. Fu, D. Zhou, Y. Tian, Y. Hu, Z. Zheng, and L. Zhou, Ceram. Int. **41**, 14718 (2015).
[15] J. S. Park, Y. J. Yoo, J. S. Hwang, J.-H. Kang, B. W. Lee, and Y. P. Lee, J. App. Phys. **115**, 013904 (2014).
[16] N. Jeon, D. Rout, I. W. Kim, and S. J. L. Kang, Appl. Phys. Lett. **98**, 072901 (2011).
[17] Z. V. Gabbasova, M. D. Kuz'min, A. K. Zvezdin, I. S. Dubenko, V. A. Murashov, D. N. Rakov, and I. B. Krynetsky, Phys. Lett. A **158**, 491 (1991).
[18] S. K. Pradhan, J. Das, P. P. Rout, V. R. Mohanta, S. K. Das, S. Samantray, D. R. Sahu, J. L. Huang, S. Verma, and B. K. Roul, J. Phys. Chem. Solids **71**, 1557 (2010).
[19] I. Sosnowska, W. Schäfer, and I. O. Troyanchuk, Physica B: Condens. Matter **276**, 576 (2000).
[20] P. Suresh, P. D. Babu, and S. Srinath, J. Appl. Phys. **115**, 17D905 (2014).
[21] V. A. Khomchenko, I. O. Troyanchuk, D. M. Többens, V. Sikolenko, and J. A. Paixão, J. Phys. Condens. Matter **25**, 13 (2013).
[22] I. O. Troyanchuk, D. V. Karpinsky, M. V. Bushinsky, M. I. Kovetskaya, E. A. Efimova, and V. V. Eremenko, J. Exp. Theor. Phys. **113**, 1025 (2011).
[23] H. Singh and K. L. Yadav, J. Phys.: Condens. Matter **23**, 385901 (2011).
[24] J. Rodríguez-Carvajal, Physica B: Condens. Matter **192**, 55 (1993).
[25] J. M. Moreau, C. Michel, R. Gerson, and W. J. James, J. Phys. Chem. Solids **32**, 1315 (1970).
[26] P. Suresh and S. Srinath, IOP Conf. Series: Materials Science and Engineering **73**, 012082 (2015).
[27] S. A. T. Redfern, C. Wang, J. W. Hong, G. Catalan, and J. F. Scott, Phys. Rev. B **77**, 144403 (2008).
[28] M. Sarathbavan, K. Annamalai, T. Parida, K. Ramesh Kumar, A. M. Strydom, K. Ramamurthi, and K. Kamala Bharathi, J. Magn. Magn. Mater. **474**, 144 (2019).
[29] P. Suresh and S. Srinath, Materials Focus **2**, 201 (2013).
[30] A. S. Wills, Physica B: Condens. Matter **276**, 680 (2000).
[31] R. Haumont, P. Bouvier, A. Pashkin, K. Rabia, K. S. Frank, B. Dkhil, W. A. Crichton, C. A. Kuntscher, and J. Kreisel, Phys. Rev. B **79**, 184110 (2009).

[32]A. S. Panfilov, G. E. Grechnev, and V. M. Ishchuk, Low Temp. Phys. **41**, 528 (2015).
[33]D. Kothari, V. R. Reddy, V. G. Sathe, A. Gupta, A. Banerjee, and A. M. Awasthi, J. Magn. Magn. Mater. **320**, 548 (2008).
[34]Z. Chen, Y. Wu, X. Wang, W. Jin, and C. Zhu, J. Mater. Sci. Mater. Electron **26**, 9929 (2015).
[35]E. Kirkendall, L. Thomassen, and C. Upthegrove, Trans. AIME **133**, 186 (1939).
[36]P. Sharma and V. Verma, J. Mag. Mag. Mater. **374**, 18 (2015).
[37]E. H. Putley, *Semiconductors and semimetals* (Academic press, New York, 1970), 5, p. 259.
[38]M. Rangi, S. Sanghi, S. Jangra, K. Kaswan, S. Khasa, and A. Agarwal, Ceram. Int. **43**, 12095 (2017).
[39]K. W. Wagner, Ann. Phys. **40**, 817 (1913).
[40]C. G. Koops, Phys. Rev. **83**, 121 (1951).
[41]Reetu, A. Agarwal, S. Sanghi, Ashima, N. Ahlawat, and Monica, J. Appl Phys **111**, 113917 (2012).
[42]N. Kumar, A. Shukla, N. Kumar, R. N. P. Choudhary, and A. Kumar, RSC Adv. **8**, 36939 (2018).
[43]M. Viviani, M. Bassoli, V. Buscaglia, M. T. Buscaglia, and P. Nanni, J. Phys. D: Appl. Phys. **42**, 175407 (2009).
[44]M. Idrees, M. Nadeem, M. Atif, M. Siddique, M. Mehmood, and M. M. Hassan, Acta Mater. **59**, 1338 (2011).
[45]N. Kumar, A. Shukla, and R. N. P. Choudhary, J. Alloy Compd. **747**, 865 (2018).
[46]Y. Ma and X. M. Chen, J. Appl. Phys. **105**, 054107 (2009).
[47]T. D. Rao and S. Asthana, J Appl. Phys. **116**, 164102 (2014).
[48]N. Kumar, A. Shukla, N. Kumar, R. N. P. Choudhary, S. Sahoo, and S. Hajra, Ceram. Int. **45**, 822 (2019).
[49]N. Kumar, A. Shukla, and R. N. P. Choudhary, Pro Nat Sci-Mater **28**, 308 (2018).
[50]S. Rani, S. Sanghi, A. Agarwal, and N. Alhawat, J Alloys Compd. **619**, 659 (2015).
[51]T. Bhasin, A. Agarwal, S. Sanghi, R. K. Kotnala, J. Shah, M. Yadav, M. Tuteja, and J. Singh, Mater. Res. Express **5**, 106102 (2018).
[52]A. R. James, S. Priya, K. Uchino, and K. Srinivas, J. Appl. Phys. **90**, 3504 (2001).